Neurobiology of Disease

Spatially Patterned Electrical Stimulation to Enhance Resolution of Retinal Prostheses

Lauren H. Jepson,[1,2] Paweł Hottowy,[3] Keith Mathieson,[4] Deborah E. Gunning,[4] Władysław Dąbrowski,[3] Alan M. Litke,[5] and E. J. Chichilnisky[1,6]

[1]Systems Neurobiology Laboratories, Salk Institute for Biological Studies, La Jolla, California 92037, [2]Bioengineering Department, University of California, San Diego, La Jolla, California 92093, [3]AGH University of Science and Technology, Faculty of Physics and Applied Computer Science, 30-059, Krakow, Poland, [4]Institute of Photonics, SUPA, University of Strathclyde, Glasgow G4 0NW, United Kingdom, [5]Santa Cruz Institute for Particle Physics, University of California, Santa Cruz, Santa Cruz, California 95064, and [6]Department of Neurosurgery and Hansen Experimental Physics Laboratory, Stanford University, Stanford, California 94305

Retinal prostheses electrically stimulate neurons to produce artificial vision in people blinded by photoreceptor degenerative diseases. The limited spatial resolution of current devices results in indiscriminate stimulation of interleaved cells of different types, precluding veridical reproduction of natural activity patterns in the retinal output. Here we investigate the use of spatial patterns of current injection to increase the spatial resolution of stimulation, using high-density multielectrode recording and stimulation of identified ganglion cells in isolated macaque retina. As previously shown, current passed through a single electrode typically induced a single retinal ganglion cell spike with submillisecond timing precision. Current passed simultaneously through pairs of neighboring electrodes modified the probability of activation relative to injection through a single electrode. This modification could be accurately summarized by a piecewise linear model of current summation, consistent with a simple biophysical model based on multiple sites of activation. The generalizability of the piecewise linear model was tested by using the measured responses to stimulation with two electrodes to predict responses to stimulation with three electrodes. Finally, the model provided an accurate prediction of which among a set of spatial stimulation patterns maximized selective activation of a cell while minimizing activation of a neighboring cell. The results demonstrate that tailored multielectrode stimulation patterns based on a piecewise linear model may be useful in increasing the spatial resolution of retinal prostheses.

Introduction

Retinal prostheses are designed to restore visual function to patients blinded by photoreceptor degenerative diseases, such as retinitis pigmentosa and age-related macular degeneration. Epiretinal prostheses achieve this by injecting current pulses through an array of electrodes implanted on the inner surface of the retina, to activate retinal ganglion cells (RGCs), the neurons that transmit visual information to the brain (Dagnelie, 2012). Although present-day devices produce artificial vision in blind patients, the percepts they induce are variable (Nanduri et al., 2008, 2012; Klauke et al., 2011; Pérez Fornos et al., 2012) and support only limited visual function (Richard et al., 2008; Klauke et al., 2011; Barry and Dagnelie, 2012; Humayun et al., 2012; da Cruz et al., 2013; for review of on subretinal implants, see Wilke et al., 2011; Stingl et al., 2013).

A major problem with current epiretinal prostheses is that they induce un-natural patterns of retinal activity. In a healthy retina, different features of the visual scene are transmitted to the brain by temporal patterns of activity in ~20 different RGC types that are spatially intermixed (Dacey, 2004). As a result, RGCs that are near one another often transmit very different signals. However, the large electrodes (100–520 μm in diameter; de Balthasar et al., 2008; Klauke et al., 2011; Keserü et al., 2012; Pérez Fornos et al., 2012) in current clinical prostheses likely activate hundreds or thousands of RGCs simultaneously over a region. This coarse activation not only limits the spatial resolution of artificial vision, but also generates activity that is very different from the cell type-specific activity present in a healthy retina.

An ideal prosthesis would faithfully reproduce natural spatiotemporal patterns of activity in RGCs of different types, a task that requires the capacity to independently activate each RGC. Previous work on isolated retina, using electrode arrays with much higher density and smaller electrodes than clinical prostheses, indicates that single-cell selectivity is possible for some RGCs. However, some RGCs could not be selectively activated, even in

Received July 5, 2013; revised Jan. 4, 2014; accepted Jan. 30, 2014.

Author contributions: L.H.J., P.H., W.D., A.M.L., and E.J.C. designed research; L.H.J., P.H., K.M., D.E.G., and E.J.C. performed research; L.H.J. and E.J.C. analyzed data; L.H.J. and E.J.C. wrote the paper.

This work was supported by NIH Grant R01EY021271 (E.J.C.), a Sanofi-Aventis Discovery Grant (E.J.C.), the Salk Institute for Biological Studies (L.H.J. and E.J.C.), the Joseph Alexander Foundation (L.H.J. and E.J.C.), National Science Foundation Grant PHY-0750525 (A.M.L.), National Institutes of Health Grant 5R21EB004410 (A.M.L.), the McKnight Foundation (A.M.L. and E.J.C.), Engineering and Physical Sciences Research Council (EPSRC) Grant EP/E039731/1 (D.E.G.), a Royal Society of Edinburgh fellowship (K.M.), a Research Councils UK-funded SU2P fellowship (K.M.), Engineering and Physical Sciences Research Council Grant GR/R89189/01 (K.M.), and the Polish Ministry of Science and Higher Education and its grants for Scientific Research (W.D.). We thank Matthew Grivich for software development; Clare Hulse for technical assistance; Tomasz Fiutowski, Sergei Kachiguine, Andrzej Skoczen, and Alexander Sher for technical development; Steve Barry for machining; Rich Krauzlis, John Reynolds, Mike Taffe, Ed Callaway, Tom Albright, and Howard Fox for access to primate retinas; and Martin Greschner, Jeff Gauthier, Peter Li, and Greg Field for useful discussions.

The authors declare no competing financial interests.

Correspondence should be addressed to Lauren H. Jepson, Dexcom, 6340 Sequence Drive, San Diego, CA 92121. E-mail: lhjepson@gmail.com.

DOI:10.1523/JNEUROSCI.2882-13.2014

 0270-6474/14/344871-11$15.00/0

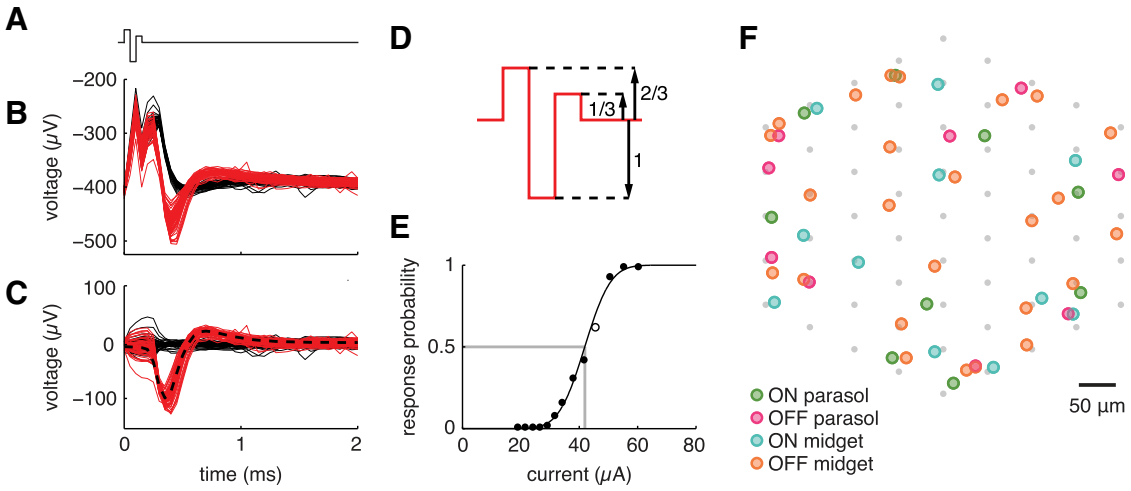

Figure 1. Analysis of RGC responses to electrical stimulation. ***A***, Waveform of triphasic current pulse applied through a single electrode. ***B***, Raw voltage traces recorded from an OFF parasol cell on the stimulus electrode during and after 100 stimulation trials in which the pulse was applied. Red traces denote trials containing a spike (successes) and black traces denote trials not containing a spike (failures). ***C***, The same data, after subtracting the average electrical artifact trace (mean of failures). Dashed black line shows the average spike waveform of the RGC recorded during visual stimulation. ***D***, Triphasic current pulse waveform with relative phase amplitudes indicated. ***E***, Probability of a spike as a function of pulse amplitude, and sigmoidal response curve fit. Open circle denotes stimulus amplitude applied in ***B*** and ***C***. Activation threshold (spike probability, 0.5) is depicted with a gray line. ***F***, Locations of cells stimulated and recorded in a single preparation. The triangulated locations of the cell bodies of stimulated cells (colored dots) are shown in relation to the array of electrodes (gray dots) used for stimulation. Different cell types are indicated by different colors.

regions of retina with relatively low ganglion cell density (Hottowy et al., 2012; Jepson et al., 2013). Thus, although increases in electrode density and decreases in electrode size may enhance the selectivity of clinical devices, additional methods will likely be required to approach single-cell selectivity, particularly in the central retina where RGC density is high.

A possible approach to this problem is to pass current through multiple electrodes simultaneously in patterns designed to enhance selectivity. This approach, sometimes referred to as "current steering" or "current focusing," has been used with some success in a range of neural stimulation devices to more precisely control the region of activation (Townshend and White, 1987; Sweeney et al., 1990; Bonham and Litvak, 2008; Butson and McIntyre, 2008; Martens et al., 2011; Habib et al., 2013; Matteucci et al., 2013). However, it is unclear whether this approach can be used to predictably alter neural responses at scales that approach single-cell resolution.

Here we demonstrate that fine-scale spatial patterns of stimulation can be used to predictably modify the firing of individual RGCs. We propose and test a simple empirical model to describe how current pulses passed simultaneously through multiple electrodes combine to activate RGCs. Finally, we show an example in which the empirical model can be used to accurately predict patterns that optimize selectivity.

Materials and Methods

Experimental setup. Multielectrode recording and stimulation were performed in a preparation of isolated primate retina as described previously (Field et al., 2007; Sekirnjak et al., 2008). Briefly, the eyes of terminally anesthetized macaque monkeys (*Macaca* species, either sex) were removed and immediately hemisected in room light. After removing the anterior portion of the eye and the vitreous humor, the posterior portion of the eye was maintained in darkness in oxygenated bicarbonate-buffered Ames' solution (Sigma). Under infrared illumination, patches of retina (~1–2 mm diameter) were isolated and placed with the RGC side down on a custom multielectrode array (MEA). A dialysis membrane placed on the photoreceptor side of the retina held the retina in place against the MEA. Dim red illumination was used briefly (<5 min) while mounting the MEA in the electrical stimulation and recording system. Throughout the experiment, the retina was superfused with Ames' solution at ~33°C. In total, data were collected from 10 preparations at eccentricities ranging from 7.5 to 14 mm (33.8–66.5° eccentricity; 33.8–61.0° temporal equivalent eccentricity), obtained from 10 macaque monkeys (Drasdo and Fowler, 1974; Chichilnisky and Kalmar, 2002). The eccentricity of one of the preparations could not be determined directly, but the measured density of ON parasol RGCs was approximately consistent with preparations from 8 mm temporal equivalent eccentricity.

A custom 64-channel multichannel electrical stimulation system (Hottowy et al., 2008, 2012) was used in conjunction with MEAs to electrically stimulate and record. Voltage recordings were bandpass filtered between 43 and 2000 Hz or 43 and 5000 Hz (−3 dB), and were amplified and digitized at 20 kHz for off-line analysis. The MEAs consisted of 61 approximately hexagonally packed (Fig. 1*F*) indium tin oxide electrodes on a glass substrate, electroplated with platinum black (Litke, 1998; Sekirnjak et al., 2006). Platinized electrodes ranged from ~9 to 15 μm in diameter. Electrodes within each row were spaced either 30 or 60 μm apart, with 30 or 60 μm between rows, resulting in center-to-center distances of either 30–33.5 or 60–67 μm.

Electrical stimulation. Current pulses were injected through individual electrodes or multiple independently controlled electrodes. Artifact reduction circuitry built into the stimulation and recording system prevented saturation of recorded voltages during and after pulse application (Hottowy et al., 2008). Charge-balanced triphasic current pulses with 50 or 100 μs phase widths and relative phase amplitudes of 2:−3:1 were chosen to further minimize electrical artifacts (Fig. 1*A*,*D*), permitting detection of low-latency (<1 ms) RGC responses on all electrodes including the electrodes used for stimulation (Hottowy et al., 2012). All reported pulse polarities and amplitudes reflect the polarity and amplitude of the second phase, with positive values indicating cathodal currents. A ring of platinum wire around the edge of the recording chamber served as a ground.

Multielectrode stimulation patterns consisted of simultaneous current injection through two to three electrodes in chosen amplitude ratios. For each targeted RGC, a "primary" electrode was chosen. With one exception (see below), the primary electrode was the electrode that resulted in the lowest activation threshold, as identified by analyzing the responses of the RGC to single-electrode stimulation with electrodes near the estimated soma position (see Materials and Methods, Electrical image calculation). Stimulation patterns involving the primary

electrode and one or two of the neighboring ("secondary") electrodes were then generated. A spatial stimulation pattern was defined as a fixed ratio of current amplitudes passed through a particular set of electrodes. In one case, an additional cell that responded to stimulation with a primary electrode was analyzed to assess selectivity (see Fig. 6), even though one of the secondary electrodes activated this additional cell at a lower threshold.

Spatial stimulation patterns were applied over a chosen range of pulse amplitudes in 10% amplitude increments while maintaining the fixed ratio of currents between electrodes. At each amplitude step, the entire set of spatial patterns was applied in random order 50 or 100 times. Sequential stimuli associated with a particular primary electrode were applied in 30 ms intervals. When more than one primary electrode was used to generate spatial patterns in a single preparation, the patterns associated with the different primary electrodes were interleaved, with either 15 ms (in the case of two primary electrodes) or 10 ms (in the case of three primary electrodes) between sequential patterns associated with different primary electrodes.

Visual stimulation. As described previously (Chichilnisky, 2001; Field et al., 2007), a spatiotemporal white noise stimulus was used to measure light response properties of RGCs. The stimulus was displayed on a cathode ray tube computer monitor, optically reduced, and focused through a microscope objective onto the photoreceptor outer segments. The stimulus was maintained at low photopic intensity with neutral density filters. Visual response data were collected for 30 min.

Spike sorting and cell type classification. Spike waveforms recorded during visual stimulation were detected and clustered into groups of spikes generated by individual RGCs, as described previously (Litke et al., 2004; Field et al., 2007). Briefly, collections of detected spike waveforms were clustered by fitting a mixture of Gaussian models after dimension reduction using principal components analysis. Clusters with a sufficient number of spikes that contained no or few refractory period violations were interpreted as representing individual RGCs.

Functionally distinct RGC types were identified based on visual response properties and electrical properties, as described previously (Field et al., 2007). Cell type identities were obtained by comparing visual response properties and cell densities to published data (Silveira and Perry, 1991; Dacey, 1993a,b, 2004; Chichilnisky and Kalmar, 2002; Dacey et al., 2003). In total, 15 cells were tested for electrical stimulation: 7 ON parasol, 4 OFF parasol, 3 ON midget, and 1 OFF midget. At the eccentricities examined, the dendritic field diameters of ON and OFF parasol RGCs range from ~150 to 225 μm, while those of ON and OFF midget cells range from ~50 to 75 μm (Watanabe and Rodieck, 1989). The approximate spacing of somas in a representative preparation (43.5° temporal equivalent eccentricity) with nearly complete recordings of these four cell types is depicted in Figure 1*F*.

Electrical image calculation. An "electrical image" (EI), indicating the average voltage waveform generated on each electrode of the MEA when a particular RGC spiked, was calculated from the spikes obtained in response to visual stimulation, as described previously (Litke et al., 2004). The EI of each RGC was used in the analysis of electrically evoked responses (see below). The EI waveforms on electrodes in the vicinity of the soma of a RGC exhibited a biphasic shape and large amplitude. Signals recorded by electrodes near the axon of a RGC had a distinct initial positive deflection, characteristic of axonal signals, and were displaced in time relative to the somatic signal as a result of spike propagation along the axon (Petrusca et al., 2007). These EI features were used to estimate soma position and axon trajectory of the cells portrayed in Figures 1*F* and 6*A*. In Figures 2*B* and 3*B–E*, the EI is represented as shaded contours generated from the waveform amplitudes across electrodes.

Analysis of electrically evoked responses. RGC responses to electrical stimuli were analyzed by categorizing waveforms recorded during trials of each stimulus pattern and amplitude as either containing only the stimulus artifact ("failures"; Fig. 1*B*, black traces) or as containing a spike from the target RGC in addition to the stimulus artifact ("successes"; Fig. 1*B*, red traces). The categorization was performed using a combination of automated and manual trace sorting, as described previously (Jepson et al., 2013). Briefly, a custom automated algorithm was used to categorize traces based on an initial estimate of the artifact waveform and the mean spike waveform recorded during visual stimulation. An updated estimate of the artifact was generated from the traces categorized as failures, and the categorization process was repeated. All results were visually inspected for errors and manually corrected when necessary. Following categorization, the electrical artifact was subtracted, revealing the uncontaminated spike waveform (Fig. 1*C*, red traces). This uncontaminated spike waveform was then compared with the EI waveform of the targeted RGC (Fig. 1*C*, black dashed line) to confirm its identity. Typically, analysis of electrically evoked responses was limited to the first 1.75 ms following pulse onset, based on the consistent observation of submillisecond response latencies (Fig. 1*C*; Sekirnjak et al., 2008; Hottowy et al., 2012; Jepson et al., 2013).

Threshold measurement. After measuring the response probability of a target RGC to a particular stimulus pattern over a range of stimulus amplitudes, a cumulative Gaussian function was fit to the data (Fig. 1*E*) using a maximum-likelihood criterion, as previously described (Jepson et al., 2013). Stimulus patterns for which the neuron did not exhibit a response probability of at least 0.4 within the analyzable current range were excluded from further analysis. Because no distinction was made between electrically evoked spikes and spontaneous spikes that occurred within the first 1.75 ms following pulse onset, calculated response rates were often nonzero, even for very low current amplitudes. To reduce the influence of these spontaneous spikes on curve fits, the fitting was performed iteratively, using only the data that fell within the range of currents corresponding to a 0.1–0.9 response probability on the sigmoidal fit and two additional data points for the currents immediately above and below this range. The threshold current was defined as the current required to elicit a response with a probability of 0.5 (Fig. 1*E*, vertical gray line), based on the curve fit.

Resampling was used to estimate the precision of the extracted thresholds. At each tested stimulus amplitude, a sample of RGC responses (successes vs failures for each stimulus trial) was drawn from the measured set of responses, with replacement. From this sample, a new response probability was calculated. A new response curve was then fit to the set of generated response probabilities, and a threshold value was extracted. This procedure was repeated 100 times, and the SD of these thresholds was taken as an estimate of threshold precision. SDs associated with each measured threshold are shown as shaded regions in Figures 2, 3, and 5. Note that these regions are often barely visible because of their size.

Linear model fitting. The linear model parameters for each electrode pair were determined by fitting a line to the thresholds obtained with the set of associated stimulus patterns. The fit was calculated by minimizing the sum of the squared perpendicular distances from each threshold to the line, in the space defined by the current passed through each electrode (Fig. 2*C–H*), using a standard nonlinear search algorithm (Nelder–Mead simplex direct search). The linear fits for each set of six electrode pairs containing the same primary electrode were constrained to intersect the axis defined by a zero secondary current at the same location (i.e., the model threshold for stimulation with the primary electrode alone) for all electrode pairs.

Nonlinearity index. A nonlinearity index was calculated to assess the quality of the linear fit for each electrode pair. The index was defined as the normalized sum of the squared distances between the linear fit and the thresholds associated with the pair, as follows:

$$\frac{1}{NR}\sum_{i}^{N} D_i^2, \quad (1)$$

where D_i is the perpendicular distance from the measured threshold for the ith stimulus pattern to the fit line, and N is the number of measured thresholds. The value of R reflects the range of threshold values measured for the electrode pair, in terms of both primary and secondary currents, as follows:

$$R = (\max(\{I_0\}) - \min(\{I_0\}))^2 + (\max(\{I_1\}) - \min(\{I_1\}))^2. \quad (2)$$

Here, $\{I_0\}$ denotes the set of thresholds in terms of the current passed through the primary electrode, and $\{I_1\}$ denotes the set of thresholds in terms of the current passed through the secondary electrode.

Piecewise linear model fitting. A piecewise linear model was fit to a subset of the electrode pair data (see Fig. 5). To avoid overfitting, only electrode pairs with a nonlinearity index $>2 \times 10^{-4}$ and with a measurable threshold to stimulation with the secondary electrode alone (either cathodal or anodal) were considered for fitting with a piecewise linear model. For electrode pairs that met these criteria, each threshold was assigned to one of the regions of stimulus space according to which set of assignments yielded the minimum value of the objective function (below), with the constraint that the set of current ratios assigned to each region constituted a sequence without gaps. The objective function was defined as the sum of squared perpendicular distances between each threshold and the portion of the piecewise linear model it was assigned to. The objective function was minimized using a Nelder–Mead simplex direct search.

Parameters were initialized in the following way. An initial estimate of the slope of each linear portion of the model was generated from a pair of measured thresholds. For the region of stimulus space containing primary-alone stimulation, the two flanking thresholds (I_i/I_0 closest to zero on either side of the axis defining primary-alone stimulation) were used, and for each region containing secondary-alone stimulation the secondary-alone threshold and neighboring threshold (highest $|I_i/I_0|$ with the same secondary electrode polarity) were used. Using these initial slope estimates, the piecewise linear model was fit separately for each electrode pair while keeping the model value for the threshold to stimulation with the primary electrode alone fixed at the measured value. The resulting parameters were used as initial parameters for fitting the set of six secondary electrodes simultaneously, allowing the value corresponding to the primary-alone threshold to vary but constraining it to be equal for all electrode pairs.

Prediction of thresholds to electrode triplet patterns. Responses to electrode triplet patterns were assessed by comparing measured activation thresholds to those predicted by the full linear model (Eq. 3), using model parameters extracted from the linear fits to electrode pair thresholds. Model predictions were calculated by setting the response probability to 0.5 (threshold), inverting the sigmoidal dependence of response probability on the stimulus, defining each secondary current as the product of the primary current and the secondary/primary current ratio used in the stimulus pattern, and solving for the primary current.

For RGCs requiring piecewise linear fitting of paired electrode responses, responses to electrode triplet patterns were predicted using model parameters associated with the region of stimulus space containing stimulation with the primary electrode alone (see Fig. 5, blue regions). As a result, the model was not expected to predict responses to triplet patterns containing I_i/I_0 ratios outside this region. These triplet patterns were excluded in all analyses of electrode triplet responses (Figs. 4 and 6). Additional data would be necessary to develop and test a model of RGC responses in these regions of stimulus space.

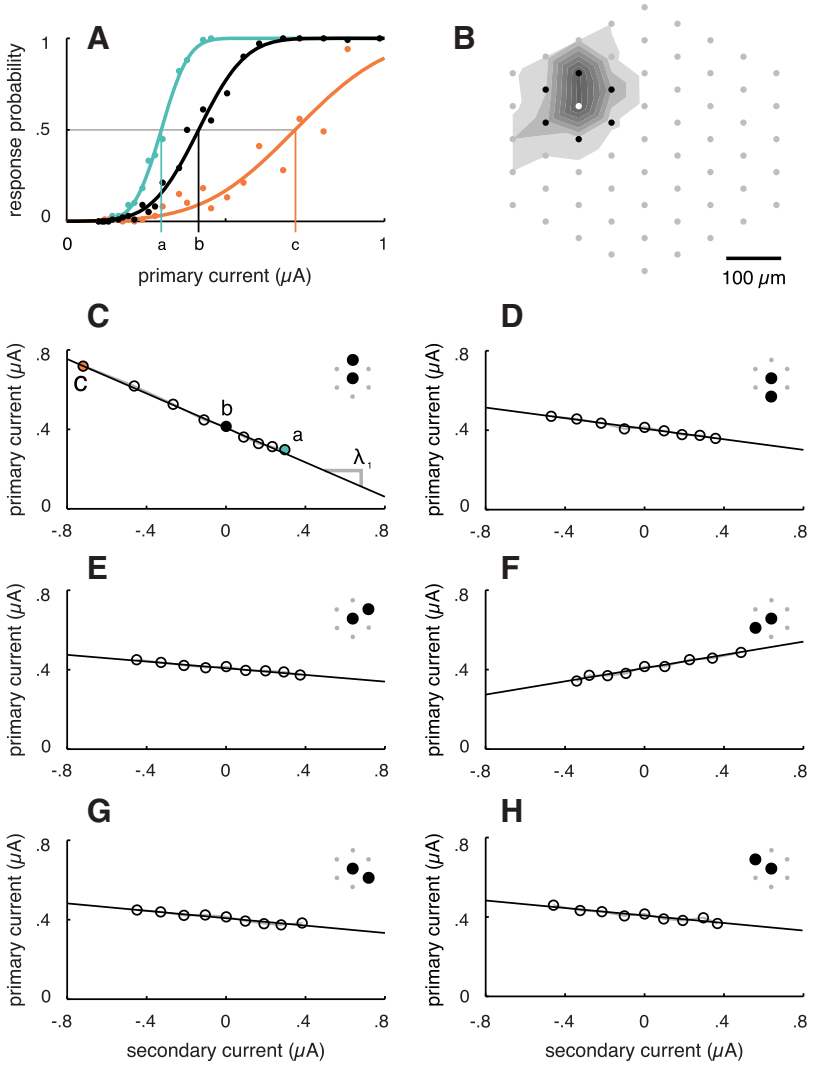

Figure 2. Linearity of current tradeoff for simultaneous current injection through pairs of electrodes. ***A***, Response curves for an OFF parasol cell (same cell as in Fig. 1*B*,*C*,*E*) resulting from cathodal current pulses injected through the primary electrode alone (black), from equal amplitude cathodal pulses passed simultaneously through one secondary electrode (teal) and from equal amplitude anodal pulses passed through the same secondary electrode (orange). Vertical lines show activation threshold for each case. ***B***, Layout of primary (white dot) and secondary (black dots) electrodes relative to the EI of the targeted RGC (shaded contours; see Materials and Methods). ***C***, Measured activation thresholds corresponding to the response curves depicted in ***A***, along with other tested current ratios for the same electrode pair (inset, black). The gray region indicates SDs of threshold estimates based on bootstrap analysis (see Materials and Methods); the width of the region is significantly smaller than the open circles. The black line depicts the linear model fit to the thresholds. Slope of the linear fit is equal to the negative of the coefficient associated with the secondary electrode (Eq. 3, λ_1). Negative secondary current values signify anodal current pulses. ***D–H***, Measured thresholds and linear model fits for the other five electrode pairs, shown in the inset (black).

Results

We used MEA recording and stimulation in isolated primate retina to probe RGC responses to fine-scale spatial patterns of current injection, and to assess the utility of these patterns for improving spatial selectivity. Experiments were focused on the four numerically dominant RGC types in the primate retina, ON parasol, OFF parasol, ON midget, and OFF midget (see Field and Chichilnisky, 2007), which collectively constitute ~70% of the visual signal transmitted to the brain in primates (Dacey, 2004). As previously observed (Fried et al., 2006; Sekirnjak et al., 2006, 2008; Tsai et al., 2009; Hottowy et al., 2012; Jepson et al., 2013), brief current pulses passed through an individual electrode of the MEA induced single, precisely timed spikes in RGCs of these types, within 1 ms of pulse onset (Fig. 1*C*). Also, the probability of

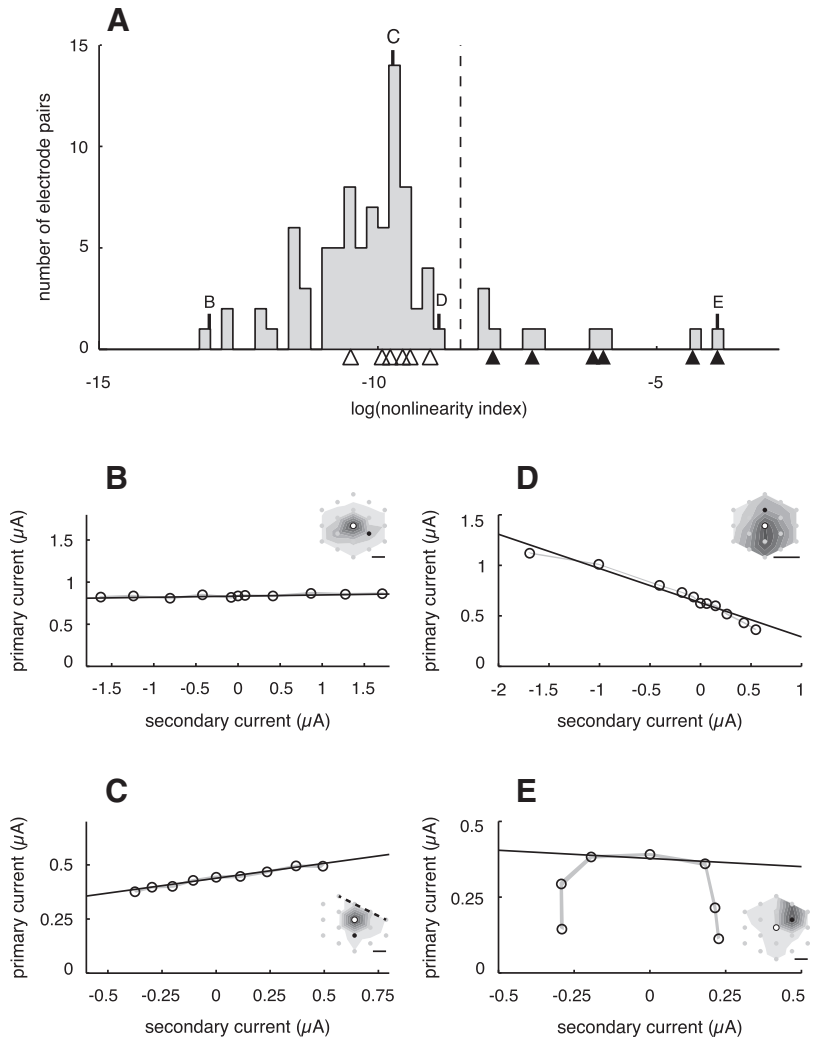

Figure 3. Linearity of current tradeoff between electrodes, with all tested electrode pairs. ***A***, Histogram of nonlinearity indices (see Materials and Methods), for all 15 cells tested (7 ON parasol, 4 OFF parasol, 3 ON midget, and 1 OFF midget) and 90 electrode pairs (6 per cell). Letters indicate nonlinearity indices of example electrode pairs shown in ***B–E***, open triangles correspond to electrode pairs shown in Figure 2, and filled triangles correspond to pairs shown in Figure 5. The vertical dashed line indicates the minimum nonlinearity index for which fitting with a piecewise linear model was attempted (see Materials and Methods and Results, Piecewise linear model fitting). ***B–E***, Measured thresholds and linear fits of four electrode pairs, illustrating the range of observed degrees of linearity. Shaded regions depict SDs of threshold estimates based on bootstrap analysis (see Materials and Methods). Insets indicate electrical image of targeted cell (see Materials and Methods) and electrodes used for stimulation; white is primary, black is secondary. Dashed line in ***C*** indicates the edge of the electrode array. Horizontal scale bars, 50 μm. Positive and negative current values signify cathodal and anodal pulses, respectively. ***B***, ON midget cell. ***C***, ON midget cell. ***D***, OFF parasol cell. ***E***, ON parasol cell.

response increased with increasing pulse amplitude, following a sigmoidal curve (Fig. 1*E*; Sekirnjak et al., 2008; Fried et al., 2009; Tsai et al., 2009; Hottowy et al., 2012; Jepson et al., 2013).

Responses to electrode pairs

To investigate the utility of patterned stimulation, current was passed simultaneously through a second electrode, with the same waveform and polarity. This manipulation generated RGC responses that were qualitatively similar to those evoked by single-electrode stimulation. However, the current passed through the second electrode typically caused a decrease in the current through the first electrode required to elicit a spike, producing a leftward shift in the response curve (Fig. 2*A*, teal curve vs black curve). Conversely, an opposite polarity current passed through the second electrode caused an increase in the current through the first electrode required to elicit a spike, producing a rightward shift in the response curve (Fig. 2*A*, orange curve vs black curve). These shifts were quantified in terms of changes in threshold, which was defined as the current required on the original electrode to elicit a spike with probability 0.5 (Fig. 2*A*).

Linear model of current combination

The above effects of additional stimulation electrodes provide a potential strategy for increasing selectivity. For example, an appropriate combination of currents passed through multiple electrodes could increase the response probability of a targeted RGC and/or decrease the response probability of neighboring RGCs, relative to single-electrode stimulation (see Fig. 6). However, determination of the most selective stimulation pattern requires an understanding of how currents from multiple electrodes combine to influence the responses of RGCs. The simplest and most computationally tractable hypothesis is that currents combine linearly, as follows:

$$P = f(I_0 + \lambda_1 I_1 + \lambda_2 I_2 + \ldots + \lambda_n I_n), \quad (3)$$

where P is the probability of the RGC response; f is the sigmoidal dependence of response probability on stimulus amplitude; $I_0, I_1, I_2, \ldots, I_n$ denote the amplitude and polarity of the current pulse applied through each electrode; and $\lambda_1, \lambda_2, \ldots, \lambda_n$ describe the relative strength and polarity of the influence of each electrode.

To test the linear model, RGC responses to current passed through pairs of electrodes were examined. For each RGC, a primary stimulation electrode was first chosen (see Materials and Methods). A set of spatial stimulation patterns involving this electrode and each of the six neighboring secondary electrodes was then tested, over a range of amplitudes and with a fixed ratio of currents between the two electrodes (Fig. 2*C–H*, insets). In total, 15 RGCs from 10 retina preparations were investigated, with 6–10 current ratios tested on each of the 6 electrode pairs for each cell.

The key empirical prediction of the linear model is that currents passed through different electrodes trade off in fixed proportion to influence firing. If this is correct, the collection of thresholds associated with a particular electrode pair would be expected to fall along a line in the stimulus space defined by the currents passed through the two electrodes. Figure 2*C–H* shows the measured thresholds (open circles) of one RGC to six tested electrode pairs, superimposed on linear fits for each pair. The accuracy of the fits supports the linear model hypothesis. Different secondary electrodes influenced responses to varying degrees, resulting in different slopes (Fig. 2*C–H*), as would be expected for

electrodes located at different distances from the cell. In most cases, passing same-polarity (cathodal) pulses through a secondary electrode decreased the threshold, whereas opposite polarity (anodal) pulses resulted in threshold increases (Fig. 2*C–E*,*G*,*H*). The opposite effect was observed in some cases (Fig. 2*F*; see Discussion), but the dependence of the threshold on secondary electrode current remained linear.

Overall, the tradeoff in currents required to achieve threshold activation for the majority of tested electrode pairs was accurately described by a linear model (Figs. 2*C–H*, 3*B*,*C*). To quantify this observation, a nonlinearity index was calculated for each electrode pair: the normalized sum of squared differences between the thresholds and the linear fits (see Materials and Methods). The nonlinearity indices for all tested electrode pairs are shown as a histogram in Figure 3*A*; the electrode pairs from Figure 2 are indicated with open triangles. The vast majority of tested pairs exhibited a similar degree of linearity to the electrode pairs depicted in Figure 2, although in a few cases, slight curvature was observed (Fig. 3*D*). A small number of pairs exhibited much higher indices, indicating more nonlinear current tradeoffs (Fig. 3*E*). These exceptions will be discussed below.

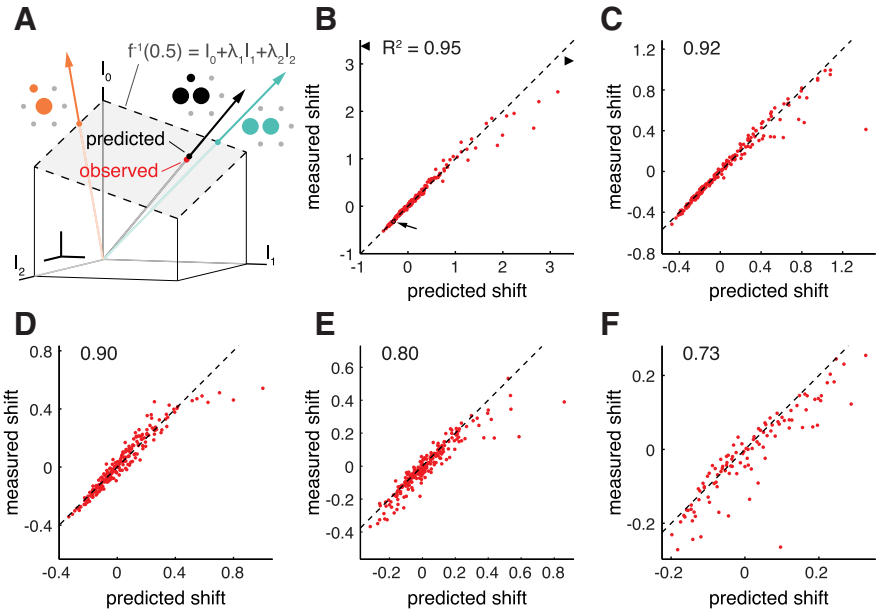

Figure 4. The linear model accurately predicts threshold shifts resulting from stimulation with electrode triplet patterns. ***A***, Depiction of activation threshold as a linear function of currents passed through three electrodes (gray plane, equation), for an ON parasol cell. Vectors show currents associated with a tested triplet pattern (black) and the two pair patterns with the same secondary/primary current ratios as was used in the triplet pattern (orange and teal). Neighboring schematics depict current ratios (represented as diameters of circles) corresponding to each pattern. Threshold predictions lie at the intersection of each vector and the threshold plane. Measured threshold is shown in red. Inset scale bars, 0.1 μA. ***B–F***, Comparison of observed and predicted thresholds to electrode triplet patterns for each of the five tested RGCs. Triplet pattern depicted in ***A*** is marked with an arrow and a small black outline in ***B***. Thresholds are plotted as fractional shifts from the model value for primary-alone threshold ($f^{-1}(0.5)$ in Eq. 3). Dashed black lines indicate 1:1 correspondence between predicted and measured values. Coefficients of determination (R^2), indicating the proportion of measured variance in the data that is explained by the linear model, are shown in the top left of each panel. Two data points outside the range of the horizontal axis in ***B*** are shown as triangles at the axis limits. These two data points correspond to patterns containing high secondary/primary current ratios, which frequently require a piecewise linear model to describe (see below), and are therefore excluded from calculation of R^2. ***B***, ***C***, ON parasol cells. ***D***, ON midget cell. ***E***, OFF parasol cell. ***F***, ON parasol cell.

Extension to electrode triplets

In principle, groups of three or more electrodes could be even more effective than pairs of electrodes at improving selectivity. The full linear model (Eq. 3) predicts a linear tradeoff between the currents injected by an arbitrary number of electrodes on activation thresholds. In the case of electrode triplets, the model predicts that the threshold shifts induced by each of the two secondary electrodes should be additive (Fig. 4*A*).

This tk;4prediction was tested by measuring the responses of RGCs to current passed through electrode triplets consisting of the primary electrode and pairs of neighboring secondary electrodes. The resulting thresholds were compared with the thresholds predicted by the model, based on the parameters estimated from paired electrode stimulation (see Materials and Methods).

The model prediction of responses to electrode triplets was tested in five cells (Fig. 4*B–F*). Although some deviations from linearity were observed, the measured thresholds generally were captured by the linear model, with coefficients of determination (R^2) ranging from 0.73 to 0.95.

Piecewise linear model

A subset of the examined electrode pairs exhibited highly nonlinear current tradeoffs (Fig. 3*E*). In most cases, the observed nonlinearities could be accounted for by using a piecewise linear model: dividing the stimulus space into regions and fitting a separate linear model to thresholds within each. Piecewise linearity is consistent with the existence of distinct linear current tradeoffs in different regions of stimulus space, corresponding to spike initiation at different locations on the cell membrane or different times relative to the stimulus (see Discussion).

Example of increased selectivity

Spatial stimulation patterns have the potential to increase selectivity by producing an electric field optimized for activating one cell more strongly than others. The utility of this approach was tested by comparing the activation thresholds of a pair of neighboring RGCs, an OFF parasol cell (target; Fig. 6*A*, green) and an ON parasol cell (nontarget; Fig. 6*A*, gray), to various stimulation patterns. First, the selectivity achievable using single-electrode stimulation with the primary electrode and each of the six surrounding secondary electrodes was assessed. Each electrode that elicited a target cell spike within the tested current range either activated both cells approximately equally (Fig. 6*B*), or preferentially activated the nontarget cell (Fig. 6*C*,*D*). Thus, single-electrode stimulation could not selectively activate the target cell.

Next, selectivity using a set of two- and three-electrode spatial patterns was compared with the greatest selectivity achievable with a single electrode. A wide range of selectivities could be achieved with different patterns: the difference between target and nontarget RGC thresholds achieved with patterned stimulation ranged from 6.2 to −5.2 times the threshold difference for optimal single-electrode stimulation (Fig. 6*G*, right axis). The most selective pattern was capable of reliably activating the target cell (0.9 probability) without significantly activating the nontarget

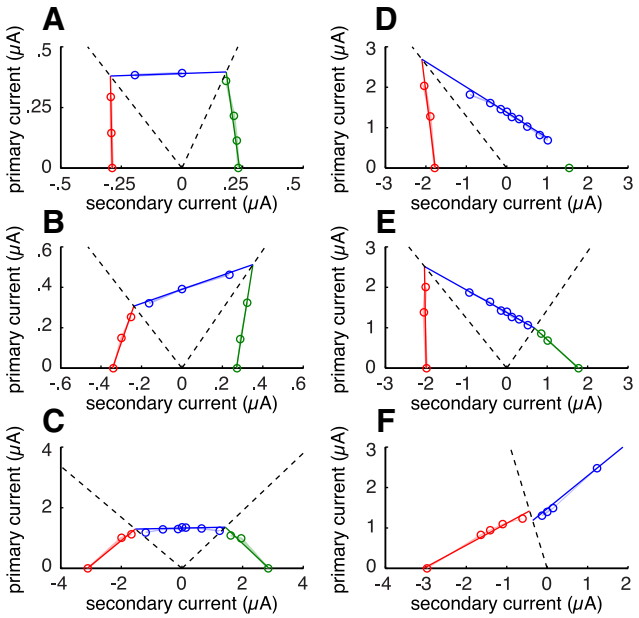

Figure 5. Piecewise linear fitting of electrode pair data exhibiting nonlinear current tradeoffs. Open circles represent measured thresholds, colored according to the region of stimulus space to which they are assigned in fitting the model; region boundaries are shown by dashed lines (see Materials and Methods). Piecewise linear model fits are shown as colored lines. Shaded regions indicate the SDs of threshold estimates from bootstrap analysis (see Materials and Methods). Positive and negative current values denote cathodal and anodal currents, respectively. ***A–E***, ON parasol cells. ***F***, OFF parasol cell.

cell (0.11 probability; Fig. 6*E*). This was substantially more selective than single-electrode stimulation, in which the current required to reliably activate the target cell also strongly activated the nontarget cell (0.98 probability; Fig. 6*B*).

In a retinal implant, it would be impractical to test all possible stimulus patterns to determine which would achieve the greatest selectivity. The piecewise linear model provides a natural way to predict the optimally selective pattern based on a limited set of measurements. This was tested on the target and nontarget RGCs examined above. First, the linear model parameters for each cell were determined by fitting the results of stimulation with pairs of electrodes. The linear model was then used to predict which of a collection of two- and three-electrode stimulation patterns would result in the greatest selectivity for the target cell, based on the predicted difference in threshold between the two cells. The selectivity of the spatial pattern that was predicted to be optimally selective (Fig. 6*F*) was nearly identical to the selectivity of the measured optimal pattern (Fig. 6*E*), allowing for 0.90 activation probability of the target cell with only 0.11 probability of activating the neighboring cell.

The overall performance of model predictions was assessed by comparing the predicted and measured selectivity of each stimulus pattern. In Figure 6*G*, the threshold difference predicted by the model is shown (black), is ordered from most to least selective for the target RGC, and is compared with the measured threshold differences (red). Although the measured threshold differences deviated slightly from the model prediction for some patterns, in general the model was a strong predictor of measured selectivity. Note that analysis of selectivity was only performed for these two cells; thus, it remains possible that other cells were activated. A more complete analysis of selectivity (Sekirnjak et al., 2008; Jepson et al., 2013) will be necessary to understand how broadly these findings will generalize.

Discussion

The present results show that a simple piecewise linear model accurately describes the responses of individual RGCs to fine-scale spatial patterns of current injection, and that these patterns could potentially provide a strategy to improve the selectivity of epiretinal stimulation in a retinal prosthesis.

Comparison with previous field-shaping studies

The utility of multielectrode stimulation patterns in providing greater spatial control of neuronal activation, often referred to as "current steering" or "current focusing," has been demonstrated at coarse spatial scales in several neural structures, from the cochlea (Townshend and White, 1987; Bonham and Litvak, 2008), to deep brain nuclei (Martens et al., 2011) and nerves (Sweeney et al., 1990). The present work, by contrast, focused on a spatial scale on the order of the size of the neurons being targeted. At this scale, it is likely that the detailed morphology and biophysics of the targeted neurons play a significant role in determining their responses to current steering. Thus, it was unclear whether current steering, which we refer to as patterned stimulation, at this scale would result in systematic, predictable changes in neural activation that would have practical utility for improving selectivity.

This study is also the first to use stimulus patterns tailored to individual cells. Previous studies in the retina have focused on global strategies, such as the use of one or more local return electrodes to confine the spread of current and thus the region of activation (Abramian et al., 2011; Habib et al., 2013; Matteucci et al., 2013), field shaping to reduce the likelihood of activating passing axons (Grumet, 1999; Rattay and Resatz, 2004; Mueller and Grill, 2013), or current steering to activate groups of RGCs between stimulation electrodes (Mueller and Grill, 2013). At the finer spatial scales examined here, tailoring the stimulation patterns to the specific morphological and biophysical properties of each targeted cell has the potential to produce greater selectivity than a global strategy. However, this potential comes at a cost. A retinal prosthesis using this approach must be able to record RGC responses to deliver tailored stimuli (see below).

The cell types examined here were selected primarily on the basis of ease of analysis in multielectrode recordings, a criterion that favored parasol cells because of spike sorting in the presence of stimulus artifact, although some midget cells were examined as well. Previous work on single-electrode stimulation thresholds (Jepson et al., 2013) and the current results on piecewise linear summation suggest that the basic properties relevant for tailored stimulation may be consistent across cell types, but further work will be required to confirm this suggestion in the diverse RGC types and across retinal eccentricities.

Biophysical interpretation of linear current tradeoffs

What is the biophysical basis for the observed linearity of current sources in activating RGCs within certain current ranges? The precise effect of current injection on neuronal activity is a complex function of several parameters, including electrode geometry, tissue electrical properties, pulse shape, neuron morphology, and membrane dynamics, and is outside the scope of this discussion (McIntyre and Grill, 1999; Rattay, 1999). However, valuable insight can be gained by considering general properties of the passive membrane response.

The passive voltage deflection produced by electrical stimulation at a particular time and location on the cell membrane is a linear function of the currents passed through the electrodes.

This is a result of two factors. First, the extracellular electric field generated by a set of current sources is a linear combination of the fields generated by each source. Second, the passive voltage deflection at any given time and location on the cell membrane is a linear function of the extracellular electric field (Barr and Plonsey, 1995). As a result, if spike initiation is approximated as occurring when the membrane potential at a particular time and location exceeds a threshold value (Warman et al., 1992), the probability of activation will be determined by a linear function of the currents passed through the electrodes (Eq. 3), consistent with the majority of the observations in this study.

This framework also provides a potential explanation for the opposite-sign current tradeoff observed for some electrode pairs; that is, a reduction rather than an increase in activation threshold upon anodal (opposite polarity) current injection through the secondary electrode (Figs. 2*F*, 3*C*). Modeled responses of neurons to single-electrode stimuli show that cathodal currents typically cause depolarization in some regions of membrane and hyperpolarization in other regions (Rattay, 1999; Rattay et al., 2003). An opposite-sign current tradeoff would be expected if the membrane at the location of spike initiation was depolarized by a cathodal pulse passed through one electrode but hyperpolarized by a cathodal pulse passed through the other electrode (Fig. 7*C*).

It is important to note that treating spike initiation as a passive membrane depolarization to a threshold value is a simplification. Comparison of passive membrane models to models incorporating full nonlinear membrane dynamics suggest that the magnitude of the passive depolarization that predicts spike initiation depends on pulse width and local membrane properties (Warman et al., 1992; Barr and Plonsey, 1995; McIntyre and Grill, 1999; Moffitt et al., 2004). However, a location and time-dependent threshold depolarization is not inconsistent with the framework presented above, which considers passive membrane potential at a single time and location. Additionally, nonlinear membrane dynamics can in some situations generate more complex behavior that is inconsistent with a linear model, such as spike initiation due to hyperpolarization-induced release of sodium channel inactivation (McIntyre and Grill, 1999; Rattay et al., 2003). The consistency of the measured RGC responses with the proposed linear

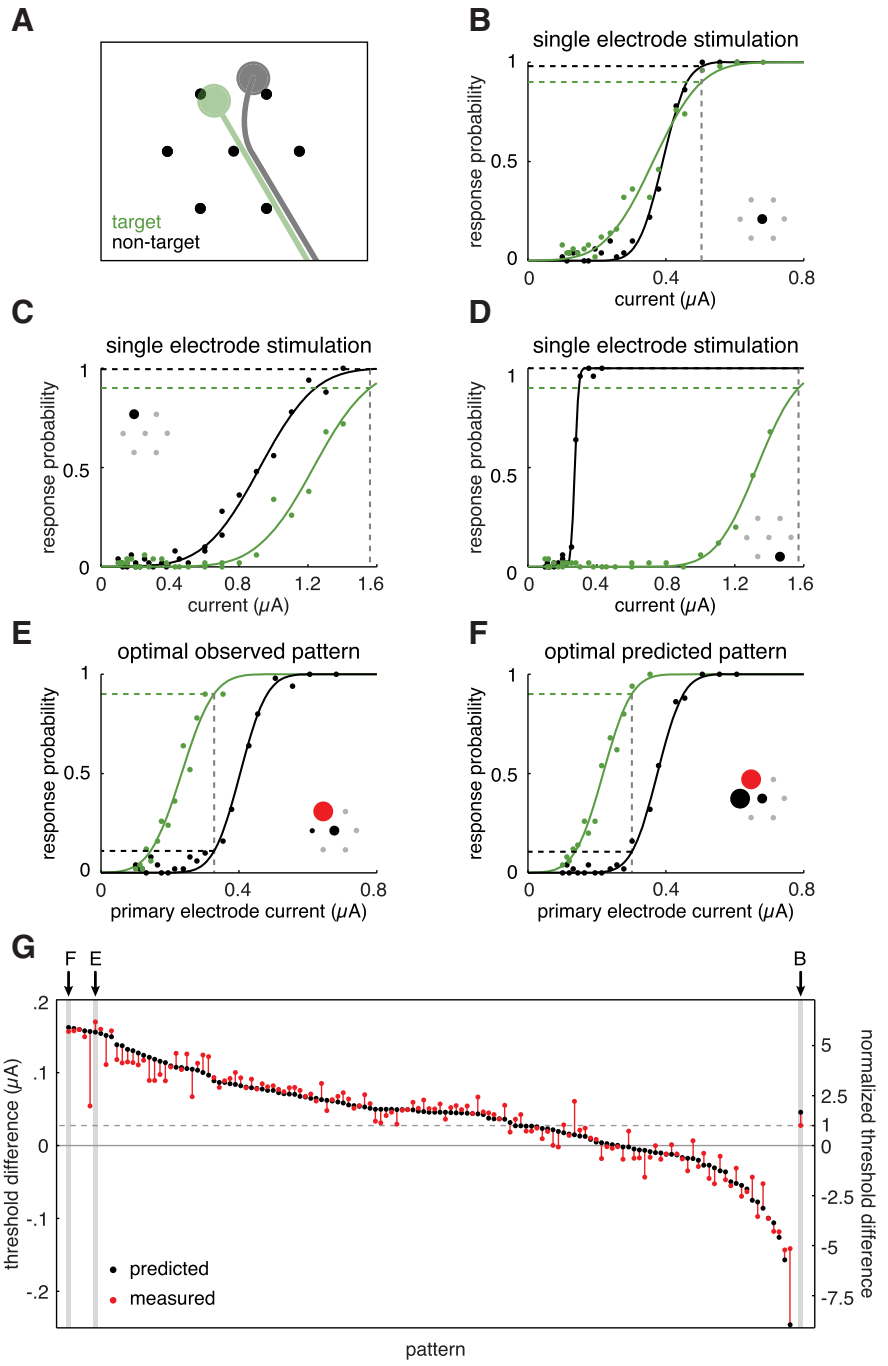

Figure 6. Activation of a target RGC (OFF parasol), without activation of a nontarget RGC (ON parasol), was not possible using single-electrode stimulation but was possible using a stimulus pattern predicted by the linear model. ***A***, Illustration of inferred soma and axon positions of target (green) and nontarget (gray) RGCs, based on the electrical image of each cell (see Materials and Methods), relative to the set of seven electrodes used in stimulation patterns. ***B–D***, Response curves for the target cell (green) and nontarget cell (black) when stimulated with each of the individual electrodes (inset) capable of eliciting a spike in the target cell. Dashed gray lines indicate the current amplitude required to activate the target cell with 0.9 probability, based on response curves. ***E***, Response curves of the target and nontarget cells for the stimulation pattern that resulted in the maximum observed selectivity for the target RGC. Selectivity was defined as the difference between the target and nontarget cell thresholds. Inset shows stimulus pattern, with circle diameters proportional to pulse amplitudes and colors indicating pulse polarity (cathodal in black, anodal in red). ***F***, Responses to stimulation with the pattern that was predicted to be maximally selective by the linear model. ***G***, Predicted (black) and measured (red) threshold differences for all tested stimulus patterns, ordered by predicted selectivity. Vertical axes indicate threshold difference in terms of primary electrode pulse amplitude (left), and normalized to the observed threshold difference of the most selective single electrode (right). ***B***, Threshold difference corresponding to stimulation with the most selective single electrode is shown for comparison at right.

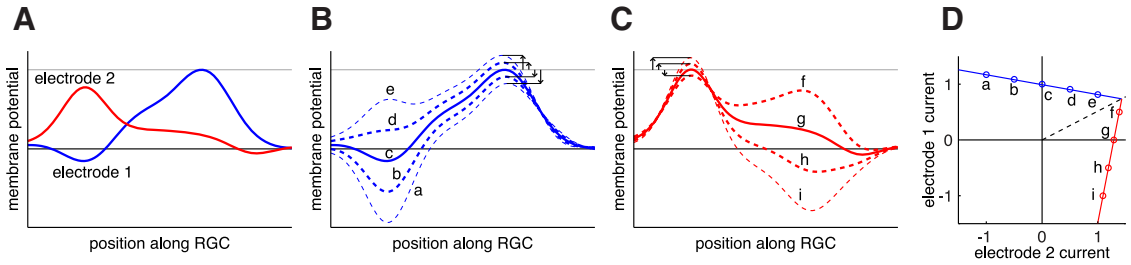

Figure 7. Biophysical interpretation of piecewise linear model, illustrated hypothetically. ***A***, Passive membrane response to a current pulse of unit amplitude injected through electrode 1 (blue) or electrode 2 (red), at a specific time relative to the stimulus. The gray line indicates hypothetical depolarization threshold for spike initiation, and the black line indicates resting potential. ***B***, Passive membrane responses to current pulse of unit amplitude injected through electrode 1 in combination with current pulses injected through electrode 2 at various amplitudes (blue): −1, −0.5, 0, 0.5, and 1 for a– e, respectively. Arrows indicate change in peak depolarization. ***C***, Passive membrane response to current pulse of fixed amplitude through electrode 2 in combination with current pulses injected through electrode 1 at various amplitudes (red): 0.5, 0, −0.5, and −1 for f–i, respectively. ***D***, Location of activation thresholds in the stimulus space defined by current passed through each electrode of the pair, based on passive membrane response profiles shown in ***A–C***. Points indicate thresholds corresponding to different currents ratios depicted in ***B*** (blue) and ***C*** (red). The dashed line shows the boundary between regions of stimulus space in which different electrodes provide the dominant depolarizing drive at the spike initiation locus. Solid lines are linear fits to thresholds within each region.

framework suggests that such nonlinear effects do not fundamentally alter the behavior of RGCs in the conditions examined.

Interpretation of piecewise linear model

Can the biophysical framework described above also provide an explanation for the piecewise linear current tradeoffs observed in some cases (Fig. 5)? Presumably, spike initiation occurs at the locus of peak depolarization within the region of the membrane capable of generating a spike, and one of the electrodes in the stimulation pattern provides the largest depolarizing drive at this locus (Fig. 7*A*, electrode 1). Current injected through other electrodes linearly alters the depolarization at this locus, which in turn linearly alters the required amount of current injected through the main driving electrode to initiate a spike (Fig. 7 *B*, *D*, blue). However, at certain current ratios, the depolarization generated by one of the other electrodes may dominate, causing the locus of activation to shift (Fig. 7*C*). The relative contribution of each electrode to depolarization at this new locus in general will be different, resulting in a different linear tradeoff between the currents passed through different electrodes (Fig. 7*D*, red). Alternatively, the spike initiation locus may shift in time rather than location. For example, certain stimulus patterns may trigger a spike at the end of the first phase of the pulse while others trigger a spike at the end of the second phase. This shift would also result in a distinct linear tradeoff because the relative contribution of each electrode to membrane polarization may be different at different times relative to the pulse.

Discrete changes in current tradeoff, reflected as "sharp corners" between regions of stimulus space (Fig. 5*A*,*B*,*E*), are predicted for discrete shifts in spike initiation locus, rather than gradual shifts. Discrete locus shifts could result from sharp, well separated peaks in depolarization generated by the separate electrodes within a pattern (Fig. 7*A*), or by the existence of discrete regions of membrane where spike initiation may occur. The "rounded corners" observed for some of the electrode pairs (Fig. 5*C*) suggest that a mixture of discrete and continuous shifts may occur. However, the piecewise linear model with discrete transitions appears to capture the majority of the observed thresholds, and provides a relatively simple basis for predicting activation thresholds based on a limited number of measurements. Thus, the model may be useful in determining optimally selective stimulation patterns (see below).

Implementation in an epiretinal prosthesis

Is it possible for a retinal prosthesis to recreate arbitrary patterns of RGC activity at the native spatial and temporal resolution of the retina? Precisely timed single spike responses to electrical stimulation have been demonstrated in previous studies in several species (Fried et al., 2006; Sekirnjak et al., 2006, 2008; Tsai et al., 2009; Hottowy et al., 2012; Jepson et al., 2013). Achieving single-cell resolution has proven more challenging. Although it is sometimes possible to activate single cells using a single electrode, unwanted activation of neighboring RGCs or passing axons has been shown to preclude selective activation in some cases (Hottowy et al., 2012; Jepson et al., 2013). This limitation is expected to be more severe in the central human retina, which has a much higher RGC density than has been examined in previous studies of selectivity (Sekirnjak et al., 2006, 2008; Hottowy et al., 2012; Jepson et al., 2013). Patterns of current delivered simultaneously through multiple electrodes, tailored for the selective activation of specific RGCs and avoidance of axon stimulation, could help to overcome this challenge.

The present results suggest a potential approach to designing optimal stimulation patterns of this kind in a future prosthesis. First, a limited set of current combinations in two or more electrodes could be applied while using the electrodes in the prosthesis to record the resulting RGC activity. Then, the recorded responses could be used to extract activation thresholds and fit a piecewise linear model for each cell. Finally, an automated optimization algorithm that exploits the piecewise linear structure of current tradeoffs could be used to compute the optimal pattern for selective stimulation of each cell. Although this approach relies on several technologies that have not yet been developed, the results presented here provide a framework for using a limited set of measurements to optimize selectivity.

References

Abramian M, Lovell NH, Morley JW, Suaning GJ, Dokos S (2011) Activation of retinal ganglion cells following epiretinal electrical stimulation with hexagonally arranged bipolar electrodes. J Neural Eng 8:035004. CrossRef Medline

Barr RC, Plonsey R (1995) Threshold variability in fibers with field stimulation of excitable membranes. IEEE Trans Biomed Eng 42:1185–1191. CrossRef Medline

Barry MP, Dagnelie G (2012) Use of the Argus II retinal prosthesis to improve visual guidance of fine hand movements. Invest Ophthalmol Vis Sci 53:5095–5101. CrossRef Medline

Bonham BH, Litvak LM (2008) Current focusing and steering: modeling, physiology, and psychophysics. Hear Res 242:141–153. CrossRef Medline

Butson CR, McIntyre CC (2008) Current steering to control the volume of tissue activated during deep brain stimulation. Brain Stimul 1:7–15. CrossRef Medline

Chichilnisky EJ (2001) A simple white noise analysis of neuronal light responses. Network 12:199–213. CrossRef Medline

Chichilnisky EJ, Kalmar RS (2002) Functional asymmetries in ON and OFF ganglion cells of primate retina. J Neurosci 22:2737–2747. Medline

Dacey DM (1993a) The mosaic of midget ganglion cells in the human retina. J Neurosci 13:5334–5355. Medline

Dacey DM (1993b) Morphology of a small-field bistratified ganglion cell type in the macaque and human retina. Vis Neurosci 10:1081–1098. CrossRef Medline

Dacey DM (2004) Origins of perception: retinal ganglion cell diversity and the creation of parallel visual pathways. In: The cognitive neurosciences (Gazzaniga MS, ed), pp 281–301. Cambridge, MA: MIT.

Dacey DM, Peterson BB, Robinson FR, Gamlin PD (2003) Fireworks in the primate retina: in vitro photodynamics reveals diverse LGN-projecting ganglion cell types. Neuron 37:15–27. CrossRef Medline

da Cruz L, Coley BF, Dorn J, Merlini F, Filley E, Christopher P, Chen FK, Wuyyuru V, Sahel J, Stanga P, Humayun M, Greenberg RJ, Dagnelie G (2013) The Argus II epiretinal prosthesis system allows letter and word reading and long-term function in patients with profound vision loss. Br J Ophthalmol 97:632–636. CrossRef Medline

Dagnelie G (2012) Retinal implants: emergence of a multidisciplinary field. Curr Opin Neurol 25:67–75. CrossRef Medline

de Balthasar C, Patel S, Roy A, Freda R, Greenwald S, Horsager A, Mahadevappa M, Yanai D, McMahon MJ, Humayun MS, Greenberg RJ, Weiland JD, Fine I (2008) Factors affecting perceptual thresholds in epiretinal prostheses. Invest Ophthalmol Vis Sci 49:2303–2314. CrossRef Medline

Drasdo N, Fowler CW (1974) Non-linear projection of the retinal image in a wide-angle schematic eye. Br J Ophthalmol 58:709–714. CrossRef Medline

Field GD, Chichilnisky EJ (2007) Information processing in the primate retina: circuitry and coding. Annu Rev Neurosci 30:1–30. CrossRef Medline

Field GD, Sher A, Gauthier JL, Greschner M, Shlens J, Litke AM, Chichilnisky EJ (2007) Spatial properties and functional organization of small bistratified ganglion cells in primate retina. J Neurosci 27:13261–13272. CrossRef Medline

Fried SI, Hsueh HA, Werblin FS (2006) A method for generating precise temporal patterns of retinal spiking using prosthetic stimulation. J Neurophysiol 95:970–978. CrossRef Medline

Fried SI, Lasker AC, Desai NJ, Eddington DK, Rizzo JF 3rd (2009) Axonal sodium-channel bands shape the response to electric stimulation in retinal ganglion cells. J Neurophysiol 101:1972–1987. CrossRef Medline

Grumet AE (1999) Electric stimulation parameters for an epi-retinal prosthesis. PhD thesis, Massachusetts Institute of Technology.

Habib AG, Cameron MA, Suaning GJ, Lovell NH, Morley JW (2013) Spatially restricted electrical activation of retinal ganglion cells in the rabbit retina by hexapolar electrode return configuration. J Neural Eng 10: 036013. CrossRef Medline

Hottowy P, Dąbrowski W, Skoczen′ A, Wiącek P (2008) An integrated multichannel waveform generator for large-scale spatio-temporal stimulation of neural tissue. Analog Integr Circuits Signal Process 55:239–248. CrossRef

Hottowy P, Skoczeń A, Gunning DE, Kachiguine S, Mathieson K, Sher A, Wiącek P, Litke AM, Dąbrowski W (2012) Properties and application of a multichannel integrated circuit for low-artifact, patterned electrical stimulation of neural tissue. J Neural Eng 9:066005. CrossRef Medline

Humayun MS, Dorn JD, da Cruz L, Dagnelie G, Sahel JA, Stanga PE, Cideciyan AV, Duncan JL, Eliott D, Filley E, Ho AC, Santos A, Safran AB, Arditi A, Del Priore LV, Greenberg RJ (2012) Interim results from the international trial of Second Sight's visual prosthesis. Ophthalmology 119:779–788. CrossRef Medline

Jepson LH, Hottowy P, Mathieson K, Gunning DE, Dabrowski W, Litke AM, Chichilnisky EJ (2013) Focal electrical stimulation of major ganglion cell types in the primate retina for the design of visual prostheses. J Neurosci 33:7194–7205. CrossRef Medline

Keserü M, Feucht M, Bornfeld N, Laube T, Walter P, Rössler G, Velikay-Parel M, Hornig R, Richard G (2012) Acute electrical stimulation of the human retina with an epiretinal electrode array. Acta Ophthalmol 90:e1–e8. CrossRef Medline

Klauke S, Goertz M, Rein S, Hoehl D, Thomas U, Eckhorn R, Bremmer F, Wachtler T (2011) Stimulation with a wireless intraocular epiretinal implant elicits visual percepts in blind humans. Invest Ophthalmol Vis Sci 52:449–455. CrossRef Medline

Litke AM (1998) The retinal readout system: an application of microstrip detector technology to neurobiology. Nucl Instrum Methods Phys Res A 418:203–209. CrossRef

Litke AM, Bezayiff N, Chichilnisky EJ, Cunningham W, Dabrowski W, Grillo AA, Grivich M, Grybos P, Hottowy P, Kachiguine S (2004) What does the eye tell the brain? Development of a system for the large-scale recording of retinal output activity. IEEE Trans Nucl Sci 51:1434–1440. CrossRef

Martens HC, Toader E, Decré MM, Anderson DJ, Vetter R, Kipke DR, Baker KB, Johnson MD, Vitek JL (2011) Spatial steering of deep brain stimulation volumes using a novel lead design. Clin Neurophysiol 122:558–566. CrossRef Medline

Matteucci PB, Chen SC, Tsai D, Dodds CW, Dokos S, Morley JW, Lovell NH, Suaning GJ (2013) Current steering in retinal stimulation via a quasi-monopolar stimulation paradigm. Invest Ophthalmol Vis Sci 54:4307–4320. CrossRef Medline

McIntyre CC, Grill WM (1999) Excitation of central nervous system neurons by nonuniform electric fields. Biophys J 76:878–888. CrossRef Medline

Moffitt MA, McIntyre CC, Grill WM (2004) Prediction of myelinated nerve fiber stimulation thresholds: limitations of linear models. IEEE Trans Biomed Eng 51:229–236. CrossRef Medline

Mueller JK, Grill WM (2013) Model-based analysis of multiple electrode array stimulation for epiretinal visual prostheses. J Neural Eng 10:036002. CrossRef Medline

Nanduri D, Humayun MS, Greenberg RJ, McMahon MJ, Weiland JD (2008) Retinal prosthesis phosphene shape analysis. Conf Proc IEEE Eng Med Biol Soc 2008:1785–1788. CrossRef Medline

Nanduri D, Fine I, Horsager A, Boynton GM, Humayun MS, Greenberg RJ, Weiland JD (2012) Frequency and amplitude modulation have different effects on the percepts elicited by retinal stimulation. Invest Ophthalmol Vis Sci 53:205–214. CrossRef Medline

Pérez Fornos A, Sommerhalder J, da Cruz L, Sahel JA, Mohand-Said S, Hafezi F, Pelizzone M (2012) Temporal properties of visual perception on electrical stimulation of the retina. Invest Ophthalmol Vis Sci 53:2720–2731. CrossRef Medline

Petrusca D, Grivich MI, Sher A, Field GD, Gauthier JL, Greschner M, Shlens J, Chichilnisky EJ, Litke AM (2007) Identification and characterization of a Y-like primate retinal ganglion cell type. J Neurosci 27:11019–11027. CrossRef Medline

Rattay F (1999) The basic mechanism for the electrical stimulation of the nervous system. Neuroscience 89:335–346. CrossRef Medline

Rattay F, Resatz S (2004) Effective electrode configuration for selective stimulation with inner eye prostheses. IEEE Trans Biomed Eng 51:1659–1664. CrossRef Medline

Rattay F, Resatz S, Lutter P, Minassian K, Jilge B, Dimitrijevic MR (2003) Mechanisms of electrical stimulation with neural prostheses. Neuromodulation 6:42–56. CrossRef Medline

Richard GK, Keserue M, Feucht M, Post N, Hornig R (2008) Visual perception after long-term implantation of a retinal implant. Paper presented at Association for Research in Vision and Ophthalmology 2008 Meeting, March-April.

Sekirnjak C, Hottowy P, Sher A, Dabrowski W, Litke AM, Chichilnisky EJ (2006) Electrical stimulation of mammalian retinal ganglion cells with multielectrode arrays. J Neurophysiol 95:3311–3327. CrossRef Medline

Sekirnjak C, Hottowy P, Sher A, Dabrowski W, Litke AM, Chichilnisky EJ (2008) High-resolution electrical stimulation of primate retina for epiretinal implant design. J Neurosci 28:4446–4456. CrossRef Medline

Silveira LC, Perry VH (1991) The topography of magnocellular projecting ganglion cells (M-ganglion cells) in the primate retina. Neuroscience 40: 217–237. CrossRef Medline

Stingl K, Bartz-Schmidt KU, Besch D, Braun A, Bruckmann A, Gekeler F,

Greppmaier U, Hipp S, Hörtdörfer G, Kernstock C, Koitschev A, Kusnyerik A, Sachs H, Schatz A, Stingl KT, Peters T, Wilhelm B, Zrenner E (2013) Artificial vision with wirelessly powered subretinal electronic implant alpha-IMS. Proc Biol Sci 280:20130077. CrossRef Medline

Sweeney JD, Ksienski DA, Mortimer JT (1990) A nerve cuff technique for selective excitation of peripheral nerve trunk regions. IEEE Trans Biomed Eng 37:706–715. CrossRef Medline

Townshend B, White RL (1987) Reduction of electrical interaction in auditory prostheses. IEEE Trans Biomed Eng 34:891–897. Medline

Tsai D, Morley JW, Suaning GJ, Lovell NH (2009) Direct activation and temporal response properties of rabbit retinal ganglion cells following subretinal stimulation. J Neurophysiol 102:2982–2993. CrossRef Medline

Warman EN, Grill WM, Durand D (1992) Modeling the effects of electric fields on nerve fibers: determination of excitation thresholds. IEEE Trans Biomed Eng 39:1244–1254. CrossRef Medline

Watanabe M, Rodieck RW (1989) Parasol and midget ganglion cells of the primate retina. J Comp Neurol 289:434–454. CrossRef Medline

Wilke R, Gabel VP, Sachs H, Bartz Schmidt KU, Gekeler F, Besch D, Szurman P, Stett A, Wilhelm B, Peters T, Harscher A, Greppmaier U, Kibbel S, Benav H, Bruckmann A, Stingl K, Kusnyerik A, Zrenner E (2011) Spatial resolution and perception of patterns mediated by a subretinal 16-electrode array in patients blinded by hereditary retinal dystrophies. Invest Ophthalmol Vis Sci 52:5995–6003. CrossRef Medline